

Study on the Thermal Decomposition Risk of 3,7-Dinitro-1,3,5,7-tetraazabicyclo[3,3,1]nonane under Different Conditions

Zhi Wang, Shaohua Jin, Guanghui Gu, Hui Chao, Shichuan Qian, Yinguang Xu, Fan Wang, Yulin Wei, Xiping Zhao, Zhiyan Lu, Shusen Chen, and Kun Chen*

Cite This: *ACS Omega* 2024, 9, 32687–32696

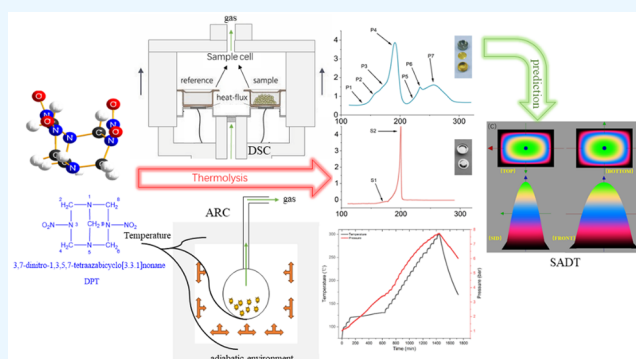
Read Online

ACCESS |

Metrics & More

Article Recommendations

ABSTRACT: Given its role as a pivotal intermediate in octogen production, the thermal safety of DPT is of paramount importance due to its significant thermal hazard. To assess the potential thermal hazard associated with its decomposition, a nonisothermal DSC experiment and an ARC test were conducted. For the acquisition of more precise thermal decomposition kinetic parameters, the impact of various crucible types on the experimental outcomes was scrutinized. The DSC results indicate that the precise thermal decomposition process of DPT, an autocatalytic decomposition material, can be accurately ascertained by using a high-pressure sealed crucible test. The authentic thermal decomposition process of DPT encompasses two critical reactions: the decomposition of DPT itself and the secondary reaction and decomposition of its byproducts. A robust thermal decomposition kinetic model was established, integrating the findings from the DSC test results. Subsequently, the risk of thermal explosion during DPT storage was simulated by using a kinetic numerical simulation approach.



1. INTRODUCTION

3,7-Dinitro-1,3,5,7-tetraazabicyclo[3,3,1]nonane (DPT), also known as dinitro pentamethylene tetramine, is a white rhombic crystal with a molecular weight of 218.2 and a density of 1.63 g/cm³. This compound serves as a critical precursor in the synthesis of octogen (HMX). There are two crystal forms of DPT, and both of them exhibit a lower impact sensitivity than that of HMX and RDX.¹ The recorded melting points are 222.0–223.0 and 204.0–205.0 °C, respectively.² DPT is soluble in acetic acid and *N,N*-dimethylformamide, but insoluble in water.³ DPT possesses an eight-membered-ring structure, and two amino groups are connected by a methylene group. The molecule exhibits structures similar to both HMX and RDX, as shown in Figure 1. DPT can be obtained by reacting sulfuric acid with hexamine dinitrate (HADN) or by nitrolysis of hexamine (HA). HMX can also be synthesized through the condensation of various nitrate amide donors with small molecules, such as formaldehyde and ammonia. The overall yield of the process ultimately determines the yield of HMX. According to the literature, nitrification of DPT can generate HMX with a yield of 75%.² Due to the nitroamine groups and the strains of the ring structure, DPT is also a potential energetic material. During storage, both the thermal stability and storage safety undergo gradual changes. This can result in a failure of the utilization and even poses a risk of

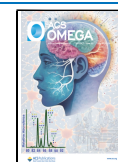
thermal explosion. In their study, Zeman^{2,5} conducted thermal decomposition tests of DPT under a nitrogen atmosphere using differential scanning calorimetry (DSC) and in an air atmosphere using differential thermal analysis (DTA). The measured initial decomposition temperature of DPT was 120.0–190.0 °C, and the heat of thermal decomposition was 117.20 ± 15.50 kJ mol⁻¹. The lower-than-expected value of the heat of decomposition was ascribed to the stability of the DPT lattice. Hall⁶ conducted a DSC test on DPT at a scanning rate of 4 K/min. The decomposition temperature was 197.9 °C, the heat of liberation was 146.50 ± 25.11 kJ mol⁻¹ and the activation energy for thermal decomposition was 418.58–1255.74 kJ mol⁻¹. Kruglyakova⁷ used liquid chromatography–mass spectrometry (LC-MS) and Duan⁸ utilized ReaxFF molecular dynamics (ReaxFF MD) simulations in conjunction with thermogravimetric-Fourier transform infrared-mass spectrometry (TG-FTIR-MS) techniques to elucidate the pyrolysis mechanism of DPT, respectively. The results indicate that the

Received: March 9, 2024

Revised: June 2, 2024

Accepted: July 3, 2024

Published: July 16, 2024



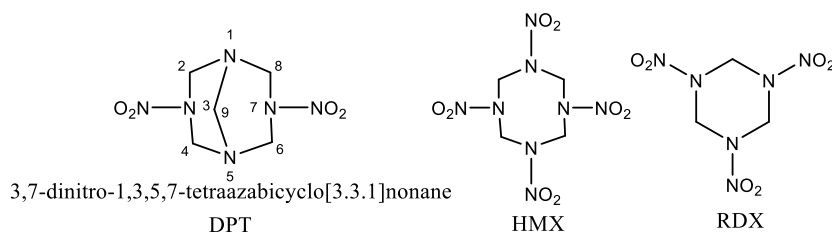


Figure 1. Structure of DPT, HMX, and RDX.

decomposition process of the DPT is highly complex, leading to the production of a large number of gaseous products. In the literature, thermal decomposition tests of DPT are often conducted in an unsealed crucible, Green⁹ proposed that these test conditions could potentially lead to misleading results and incorrect conclusions during the thermal hazard assessment process. This is particularly true for energetic materials such as DPT, where the decomposition process is an autocatalytic reaction. A significant number of gaseous products resulting from its decomposition act as catalysts in the process. When the test environment is open, this autocatalytic effect is significantly weakened, leading to oversight of its impact on safety during thermal hazard assessment. Given that the reported DPT test conditions primarily entail open systems, there is a risk of potentially misleading safety evaluations when employing DPT. In this study, we compared and analyzed the differences between the adiabatic accelerated calorimetry (ARC) test and the DSC test using an aluminum crucible with a puncture hole (Al crucible) and a high-pressure rated stainless-steel crucible (HP crucible) using a disposable gold-plated copper seal at the same scanning rate; the obtained results hold universal practical significance for the associated processes of both DPT and HMX. Afterward, the kinetics model for the thermal decomposition reaction of DPT in a sealed environment was obtained by conducting tests in a sealed crucible at various scanning rates. In the study of decomposition reaction kinetics, the constant heating rate is widely used and is a valuable tool for selective kinetic modeling in further research. Burnham¹⁰ conducted a comparison of the fitting effects of three different kinetic models on the isothermal and nonisothermal pyrolysis data of certain well-preserved algal kerogens. Jelić¹¹ employed the conversional method and model fitting approach to ascertain the optimal kinetic model fitting for ambroxol hydrochloride. The investigation revealed that ambroxol hydrochloride was not thermosensitive; however, the presence of water and crystal water facilitated its accelerated degradation. The analysis concluded that the three-parameter model exhibited superior fitting effects, thus indicating the reliability of the thermal stability conclusion. The temperature–time profiles of a specific package were simulated using thermal safety software (TSS) to predict the effects of different storage conditions. This simulation was based on a kinetic model and heat transfer conditions, specifically utilizing the thermal decomposition kinetic model. The aim was to further assess the potential risk and safety parameters of thermal damage in the event of an explosion during the transportation and storage of DPT.

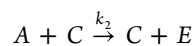
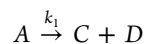
2. EXPERIMENTAL SECTION

2.1. Materials. DPT was prepared from hexamethylenetetramine by nitrolysis in a mixture of acetic anhydride and HNO₃,⁴ and the crude product was crystallized from acetone.

2.2. Methods. **2.2.1. Nonisothermal DSC Experiments.** The DSC measurement conducted on NETZSCH involved experiments under a continuous flow of nitrogen gas at a rate of 20 mL/min and the samples of DPT were weighed between 0.500 to 3.282 mg. Tests were performed using an aluminum (Al) crucible with a pierced lid and high-pressure rated stainless-steel (HP) crucibles with disposable gold-plated copper seals, respectively. And the heating rates employed were 4, 5, 6, 8, and 10 K/min.

2.2.2. ARC Experiment. The ARC measurements were conducted on an instrument manufactured by Thermal Hazard Technology Company (es-ARC). Test temperature range: 75.0–300.0 °C; Operating atmosphere: air; Test pressure range: 0–30 MPa; Detection sensitivity: 0.02 °C·min⁻¹; Test mode: H–W–S (heat–wait–seek); Heating step: 10 °C; Waiting time: 10 min; DPT was tested using Ti-LCQ bomb (10 mL, 6.07 g) and with a mass of 0.12 g.

2.3. Establishment of Thermal Decomposition Kinetics Model. The choice of the most appropriate kinetic model type is a critical stage in the creation of kinetic model creation. Burnham¹² evaluated and compared multiple global dynamic models. The autocatalytic model chosen for this study bears a resemblance to the generalized nucleation model outlined in the literature. To ensure the correctness of the results, it is essential that this stage is implemented properly.¹⁰ A comparison of the N-order and autocatalytic reaction models reveals that the autocatalytic model offers a more detailed and accurate depiction of DPT's thermal decomposition process. Consequently, this model is utilized for fitting purposes. The autocatalytic reaction is most simply described as



where substance C is the catalyst for reactant A. The total reaction rate is given by the following equation:

$$-r_A = k_1 c_A^{n_1} + k_2 c_A^{n_1} c_C^{n_2} \quad (1)$$

In the formula, r_A represents the decomposition rate of A; k_1 and k_2 are the rate constants for the elicitation and autocatalytic phases, respectively; and c_A and c_C are the concentrations of A and C at any given moment. The reaction order for A is n_1 for both phases. For C, it is n_2 during the autocatalytic phase. Equation 1 can be expressed as¹³

$$\frac{d\alpha}{dt} = A_2 e^{-\frac{E_2}{RT}} (1 - \alpha)^{n_1} \left[\left(A_1 e^{-\frac{E_1}{RT}} / A_2 e^{-\frac{E_2}{RT}} \right) + \alpha^{n_2} \right] \quad (2)$$

t represents the time in seconds; A_1 and A_2 are the pre-exponential factors for the elicitation and autocatalytic phases, respectively; α is the degree of conversion of samples. The apparent activation energies of the elicitation and autocatalytic

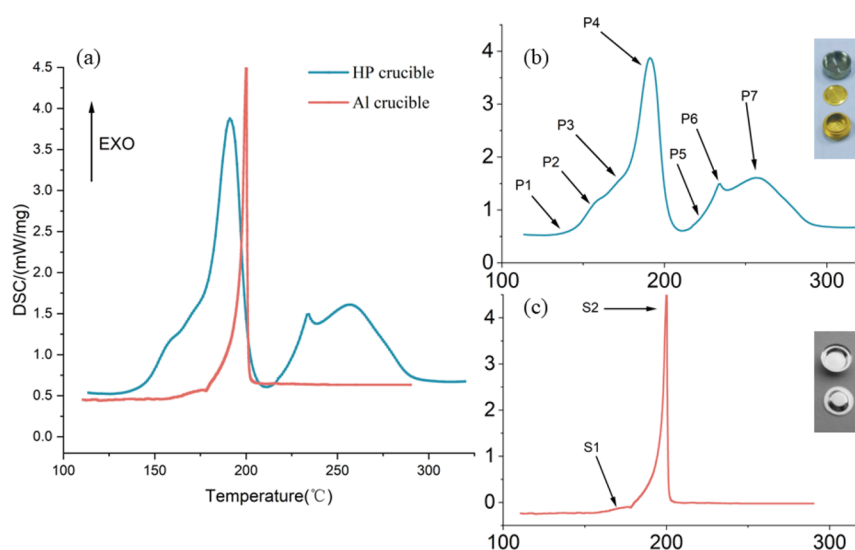


Figure 2. DSC curves: (a) DPT at different crucibles under a N_2 atmosphere with a heating rate of 5 K/min, (b) HP crucible, and (c) Al crucible

Table 1. Thermal Decomposition Parameters of DPT with a Heating Rate of 5 K/min

crucible type	initial decomposition temperature ($^{\circ}C$)		decomposition peak temp ($^{\circ}C$)		heat production J/g		E_a (kJ mol $^{-1}$)	refs
	phase 1	extrapolate onset ($^{\circ}C$)	phase 1	phase 2	phase 1	phase 2		
HP crucible	126.2	170.1	191.1	256.9	807.7 ^a	522.3 ^a		this work
Al crucible	159.4	197.1	199.9		416.6 ^a		174.1	
glass tube, sample direct contact with the air atmosphere	120.0–199.0						192.3	3
aluminum pans fitted with lids	196.0–202.0				537.2			4
crimped pans without furnace lids			197.9		671.8		221.8	5
							172.9	6
Al_2O_3 crucible with N_2 gas flow							174.6	7

^aThe heat released per unit mass of DPT from its thermal decomposition during this particular test.

phases are denoted as E_1 and E_2 , respectively. When $z_0 = A_1/A_2$ and z_0 stands for the ratio of the pre-exponential factors, as $z_0 e^{-\frac{E_z}{RT}}$ increases, the autocatalytic property becomes more intense. $E_z = E_1 - E_2$, assuming $A = A_2$ and $E = E_2$. Equation 2¹⁴ can be changed to

$$\frac{d\alpha}{dt} = Ae - \frac{E}{RT}(1 - \alpha)^{n_1} \left[z_0 e^{-\frac{E_2}{RT}} + \alpha^{n_2} \right] \quad (3)$$

The processed data are subsequently imported into the TSS software to calculate and optimize kinetic parameters.

3. RESULTS AND DISCUSSION

3.1. Effect of Different Crucible Types on the Thermal Decomposition of DPT. Under the same test conditions, using different types of crucibles with a heating rate of 5 K/min, the DSC curve is depicted in Figure 2. When tested with an Al crucible, the DSC curve shows two stages, but only one main exothermic peak (Figure 2c). In the stage of S1, DPT began to decompose and release heat slowly. A slight endothermic peak was observed, indicating the escape of decomposition gas and the removal of the heat. The temperature continued to increase, and in the stage of S2, DPT began to decompose in large quantities. The high-pressure crucible was utilized for testing. The decomposition process involved multiple exothermic stages. In the stage of P1,

DPT began to decompose slowly and produce gas products. Between the stages of P2 and P3, the gas products exhibited catalytic acceleration of the DPT decomposition reaction. In the stage of P4, DPT began to rapidly decompose under the catalysis of gaseous products. After the decomposition is completed, during stages of P5, P6, and P7, the decomposition products react with each other in a closed environment, leading to a second noticeable exothermic process. The thermal decomposition parameters obtained from the two crucible tests are given in Table 1.

By comparison, a higher initial decomposition temperature and a higher decomposition peak temperature were observed when an Al crucible was used compared to those using an HP crucible, and the decomposition process is also simpler than that using an HP crucible. As per the Zurich Hazard Analysis (Z-H-A) method,¹⁵ the average heat (Q) generated by thermal decomposition at various temperature rise rates approximated $1341.31 \pm 7.5 \text{ J g}^{-1}$, indicating the risk of the catastrophic incidence when DPT was out of control. The heat production is further reduced to only 31.32% in the high-pressure crucible. When an aluminum crucible was utilized, the results indicated a reduction in the severity of the DPT decomposition reaction to a lower level. However, for DPT, a type of energetic material with an autocatalytic decomposition reaction, the gaseous products generated by the decomposition often play a crucial role in influencing its autocatalytic characteristics.¹⁶ Therefore,

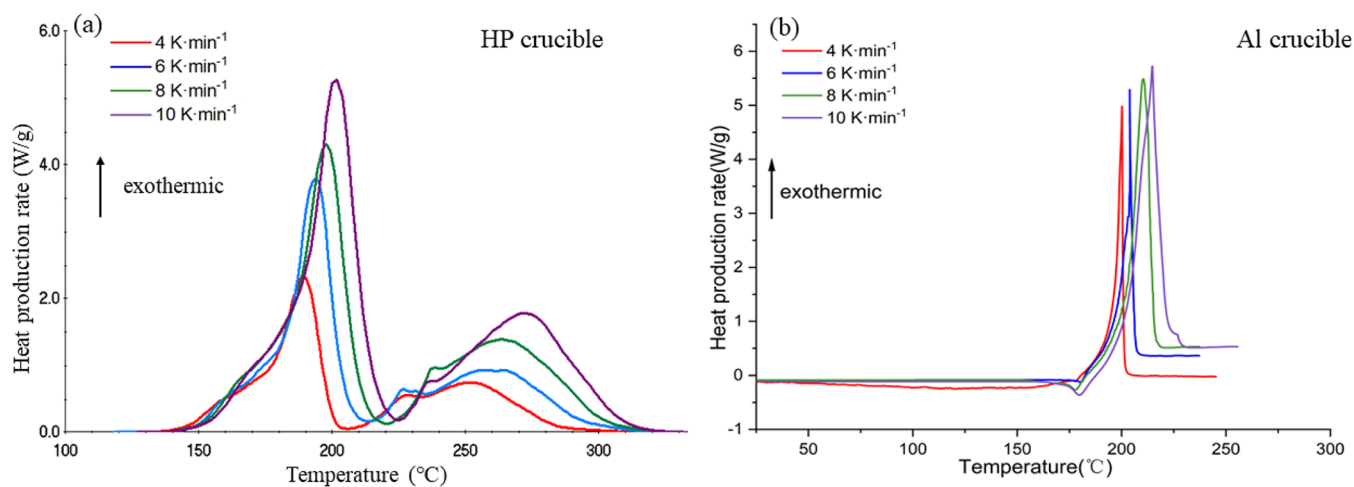


Figure 3. Nonisothermal DSC curves of DPT: (a) HP crucible and (b) Al crucible.

compared to high-pressure crucibles, aluminum crucibles cannot accurately reflect the thermal decomposition characteristics of energetic materials. Therefore, it is crucial to utilize high-pressure crucibles to measure the thermal decomposition process when dealing with energetic materials.

Figure 3 displays the rate curves of heat production from DPT thermal decomposition at different heating rates, and the corresponding experimental data were summarized in Table 2.

Table 2. Nonisothermal DSC Results of Thermodynamic Parameters

crucible type	β	sample mass (mg)	$T_{\text{onset}} (^{\circ}\text{C})$	$T_p (^{\circ}\text{C})$		$Q (\text{J g}^{-1})$	
				T_{p1}	T_{p2}	Q_1	Q_2
HP	4	3.282	138.2	189.3	252.2	806.4	536.8
	6	3.058	141.0	194.1	257.8	802.3	546.1
	8	3.003	141.4	198.0	264.2	823.8	526.2
	10	2.995	142.9	202.1	273.1	800.6	534.5
Al	4	0.68	197.1	200.2		418.8	
	6	0.65	197.9	203.9		408.2	
	8	0.52	202.0	210.5		412.2	
	10	0.50	202.2	214.7		408.7	

As heating rates increased, the exothermic peaks shift to higher temperatures, the initial decomposition temperature (T_{onset}) and peak decomposition temperature (T_p) are elevated, and the maximum heat release rates also rise.

3.2. ARC Experiment. Figure 4 shows the temperature and pressure curves of the DPT obtained during the adiabatic experiment over time. The thermal decomposition began at 120.0 °C and ended at 130.2 °C for 455 min. During the decomposition process, the pressure increases nonlinearly with the temperature. The thermal inertia factor φ is utilized to calibrate the data. The adiabatic decomposition characteristic parameters of the DPT after calibration are shown in Table 3.

Upon comparing the experimental results of ARC and DSC, it was observed that the initial decomposition temperature of DPT in ARC tests is lower, since the sample were set in an adiabatic sealed environment, and a more rapid heat accumulation occurred in the material. The initial decomposition temperature is observed to be the highest under the Al crucible test conditions because heat accumulation is

minimized during the test, and the catalytic effect of decomposition products is not significant.

3.3. Kinetic Parameter Evaluation. **3.3.1. DSC Experiment.** Although the decomposition mechanism of DPT has been studied, information regarding the secondary reaction process of the decomposed gas product has yet been reported. Therefore, a simplified kinetic model is used in this paper. The model cannot describe the detailed mechanism but can accurately depict the main characteristics of the reaction. The formal reaction models, assuming conversion degrees as state variables, are the best suited for modeling. For the exothermic decomposition of DPT, the autocatalytic reaction rate model was applied to precisely determine the kinetic parameters by fitting experimental data. Heat production rate and yield from DPT were simulated using TSS and compared with DSC experiments at heating rates of 4, 6, 8, and 10 K/min. Various apparent kinetic models were formulated to accurately depict the thermal decomposition kinetics of the DPT process. Three kinetic models consisting of 2, 4, and 7 stages, respectively, demonstrated superior fitting results and were selected. The sum of the residual squares (RSS) and Bayesian Information Criterion (BIC) values are listed in Table 4. Model comparison criteria, based on information theory, specifically the BIC,^{17,18} were utilized to determine the most suitable model. Equation 4 is employed for calculating the BIC.

$$\text{BIC} = N \ln \left(\frac{\text{RSS}}{N} \right) + K \ln (N) \quad (4)$$

where N was denoted as the number of data points, J was defined as the number of parameters to be fitted, and $K = J + 1$.

The reaction model consisting of seven stages is selected for further investigation, as it corresponds to the minimal BIC value, indicating the best model fit.

The results of the produced heat and the heat production rates are presented in Figures 5 and 6, respectively. The simulation results strongly align with the experimental data, illustrating that the reaction model effectively describes DPT's thermal decomposition. As listed in Table 5, the correlation coefficients underscore the reliability of the fitting results.

The kinetic model for the thermal decomposition of DPT measured with the HP crucible can be characterized by a dual-reaction mechanism involving seven sequential autocatalytic

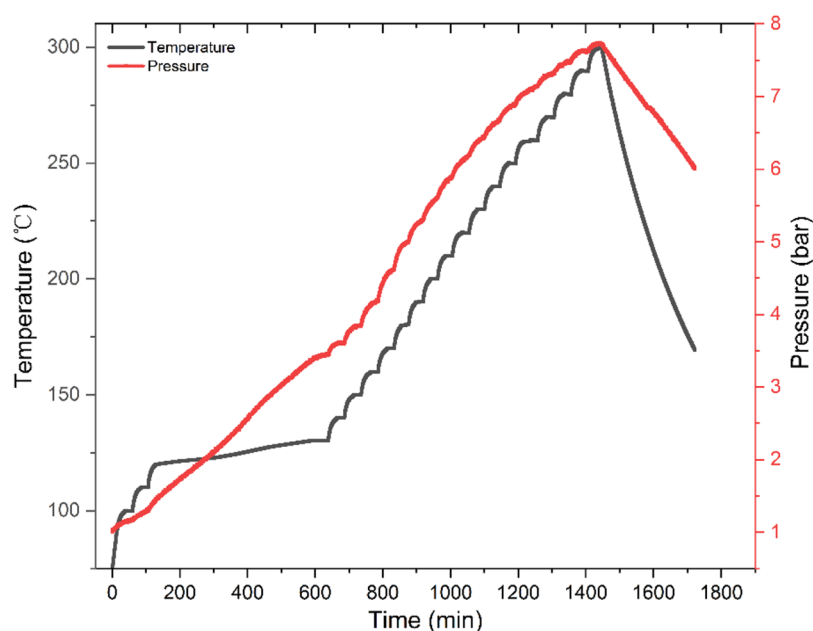


Figure 4. Curves of temperature and pressure vs time for DPT.

Table 3. Adiabatic Decomposition Characteristic Parameters

φ	initial temp rise rate (°C/min)	final decomposition temp (°C)	adiabatic temp rise (K)	max rate (°C/min)	time to reach the max temp rise rate (min)
14.03	0.022	130.2	143.8	0.047	18.96

stages. The apparent kinetic parameters for these reactions are detailed in Table 6.

When using a HP crucible, it is evident that the process is divided into two phases. Both the produced heat and the heat production rate of the first phase is higher than those of the second phase. Such an observation indicated that the decomposition becomes highly dangerous once it began. The data measured with an aluminum crucible reveal that the thermal decomposition kinetics involve a reaction with two autocatalytic decomposition stages.

The thermal decomposition mechanism is generally regarded as an inherent property of a substance,¹⁹ but the specific state of thermal decomposition under different environmental conditions is influenced by the conditions. While the kinetic model derived from DSC experiments with a constrained sample size may not be directly applicable to

industrial scales, it remains valuable for predicting and simulating thermal explosion risks. The consistency between experimental data and simulation results for both the produced heat and heat production rates confirms the utility of this model.

The stability of DPT under isothermal conditions has been simulated and predicted by utilizing kinetic parameters and equations obtained from TSS under two test conditions, characterized by time to conversion limit (TCL), the duration necessary for DPT decomposition to achieve a specific proportion at a constant temperature. Figure 7 illustrates the curves representing constant temperature against the time required to attain conversion limits of 5%, 10%, and 15%. It is evident that the duration to reach the conversion limit decreased as the temperature increased. Table 7 lists the common durations and corresponding temperatures required to achieve the three conversion limits.

The temperature corresponding to each TCL, as predicted from HP crucible test data, is lower than that obtained from the Al crucible, suggesting that DPT reaches TCL more readily and rapidly in a HP crucible. As DPT is an autocatalytic substance for decomposition, these data will provide support for evaluating the safety of DPT storage.

Simulations were conducted on the stability of DPT under adiabatic conditions to obtain the time to reach the maximum

Table 4. RSS and BIC Values for Various Models

No. of stages		heating rates (K/min)							
		4		6		8		10	
		Q^a	dQ/dt^a	Q	dQ/dt	Q	dQ/dt	Q	dQ/dt
2	RSS	29318	7645	48520	10317	18183	10635	6667	10215
	BIC	1204	892	1066	7948	711	642	502	546
4	RSS	13443	3379	30270	6106	6226	5335	7173	8558
	BIC	1061	741	614	737	614	737	542	560
7	RSS	58	45	85	133	33	127	31	193
	BIC	-48	-106	132	209	68	241	107	297

^a Q is the produced heat; dQ/dt is the heat production rate.

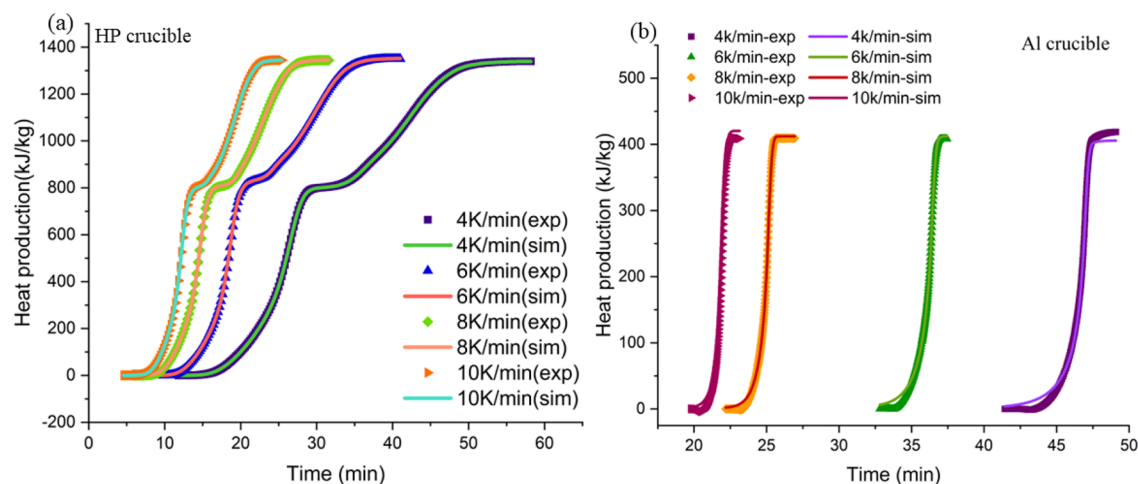


Figure 5. Experimental and simulated curves of heat production over time for DPT: (a) HP crucible and (b) Al crucible.

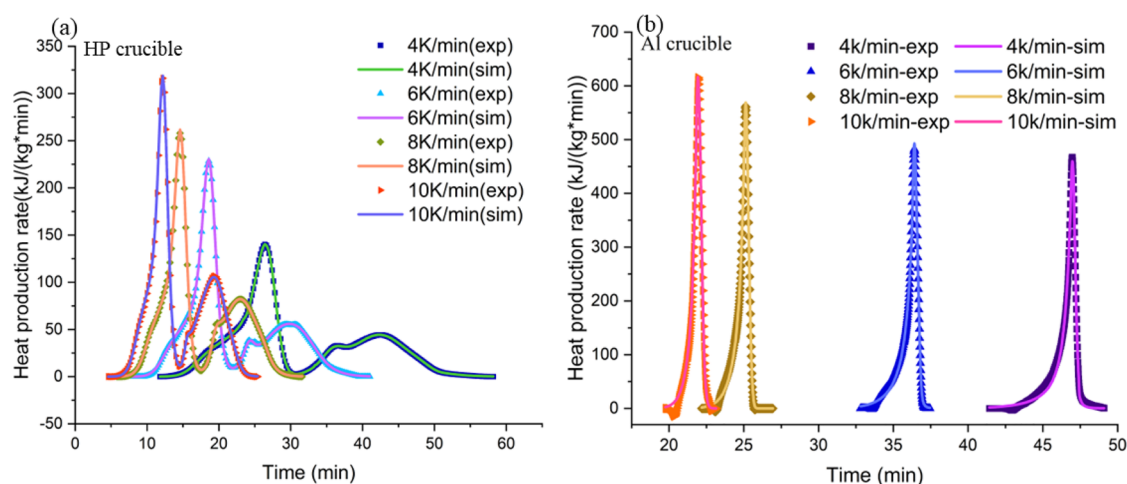


Figure 6. Experimental and simulated curves of the heat production rate over time for DPT: (a) HP crucible and (b) Al crucible.

Table 5. Correlation Coefficients of the Simulation Curves for the Produced Heats and the Heat Production Rates Measured in HP and Al Crucibles

crucible type	correlation coefficient	4k/min	6k/min	8k/min	10k/min
HP	heat production	0.9999	0.9999	0.9999	0.9999
	heat production rate	0.9999	0.9998	0.9998	0.9999
Al	heat production	0.9995	0.9997	0.9999	0.9988
	heat production rate	0.9976	0.9974	0.9985	0.9991

rate under adiabatic conditions (TMR_{ad}). As shown in Figure 8, the temperatures corresponding to the maximum reaction rates under adiabatic conditions were also obtained, respectively.

By utilization of the kinetic data derived from the HP crucible, TD_{24} of 87.2 °C and TD_8 of 96.5 °C were obtained. When DPT is stored at 87.2 and 96.5 °C, its decomposition rate under adiabatic conditions will reach its maximum value within 24 and 8 h, respectively. By utilizing the kinetic data derived from the Al crucible, TD_{24} of 127.0 °C and TD_8 of 135.0 °C were obtained, which are higher than those obtained from the HP crucible. Such result indicated the gaseous product may accelerate the decomposition of the DPT.

3.3.2. *ARC Experiment.* The thermal decomposition parameters of DPT under adiabatic conditions were calculated by curve fitting using the TSS. Figure 9 depicts the thermal decomposition experiments and the fitting results of the decomposition process. The correlation coefficients of the decomposition temperature and heat production fitting are 0.9993 and 0.9993, respectively.

Based on the apparent kinetic parameters of the reaction model (Table 8), the TMR_{ad} -temperature curve was also obtained, As shown in Figure 10. The values of TD_{24} and TD_8 are 88.5 and 98.9 °C, respectively.

When comparing the predicted TD_{24} across three test conditions, it is observed that the TD_{24} in the HP crucible aligns with the results obtained in ARC tests and is higher than that in Al crucible. Although ARC tests are conducted under adiabatic conditions, the similarity in prediction results between the two conditions can be attributed to the spacious sample bomb in ARC tests, and the less pronounced catalytic effect of decomposition products on DPT as compared to that in the high-pressure crucible.

3.4. *Analysis of Thermal Explosion and Runaway Hazards.* Given that the test utilizes granular DPT crystals, the seepage and other effects of gas in the gap are generally regarded as negligible; it is typically assumed that the reaction does not involve pore formation or phase transitions. Under

Table 6. DPT Thermal Decomposition Kinetic Parameters Derived from the TSS Simulation

crucible type	phases	stage	ln(A)	E	n ₁	n ₂	ln(Z ₀)	E _z	Q
			ln(1/s)	kJ/mol				kJ/mol	J/g
HP	phase 1	stage1	20.98	94.40	1.06	0.83	-0.95	35.02	80.92
		stage2	14.44	63.25	0.94	1.05	-0.84	21.17	185.91
		stage3	13.82	57.56	1.31	0.74	-0.11	-0.07	29.98
		stage4	16.74	54.32	0.81	0.55	-0.26	-0.09	605.33
	phase 2	stage5	19.84	99.79	2.89	0.77	-1.30	45.30	50.18
		stage6	17.41	101.10	1.02	0.01	-1.31	0.31	149.96
		stage7	12.24	73.10	0.72	0.75	-0.98	-0.48	415.59
Al	stage1	49.53	210.09	0.30	1.59	-0.74	-0.04	137.04	
	stage2	19.58	83.39	1.64	1.82	-3.12	-0.14	284.34	

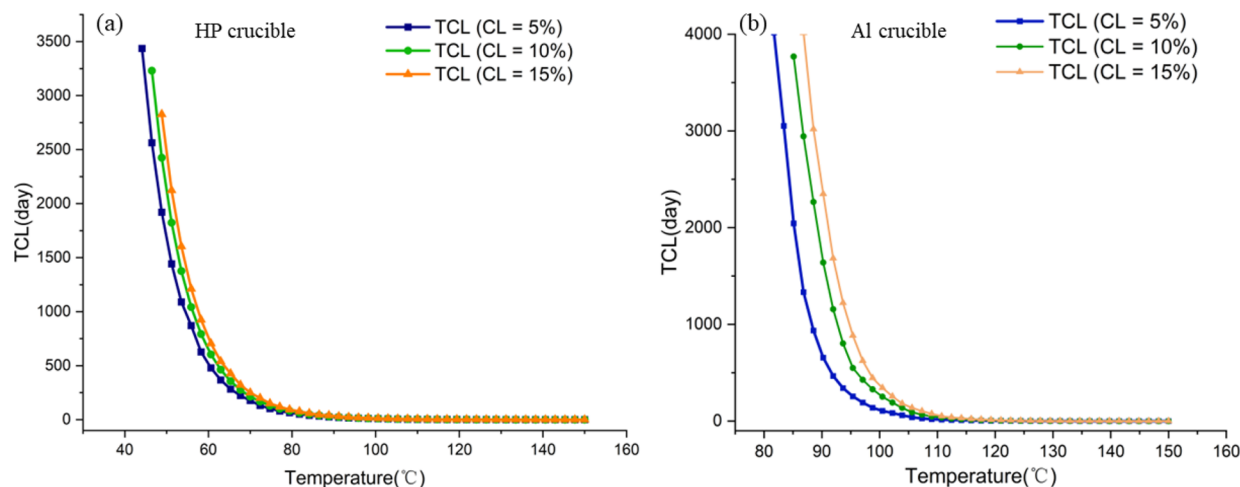


Figure 7. Time to conversion limit curves vs temperature for DPT: (a) HP crucible and (b) Al crucible.

Table 7. Common Times and Corresponding Temperatures Reach the TCL

crucible type	conversion limit (%)	exceeds 10 years	1 year	1 day
HP crucible	5	≤41.8 °C	62.9 °C	126.5 °C
	10	≤44.1 °C	65.3 °C	128.8 °C
	15	≤46.5 °C	67.7 °C	131.2 °C
Al crucible	5	≤81.7 °C	93.1 °C	127.8 °C
	10	≤83.4 °C	98.1 °C	131.3 °C
	15	≤85.1 °C	99.7 °C	134.6 °C

these conditions, heat transfer within the solid is governed by the thermal conductivity equation, which includes a nonlinear source of energy. The model for simulating thermal explosions is expressed through the following equations:^{13,20,21}

$$\rho C_p \frac{\partial T}{\partial t} = \text{div}[(\lambda(\text{grad } T))] + W \quad (5)$$

where ρ represents density, C_p stands for specific heat capacity, λ indicates thermal conductivity, W denotes thermal power, T is the temperature, and, additionally, “div” and “grad” refer to divergence and gradient, respectively. By resolving the heat equation, the temporal and spatial evolution of temperature in

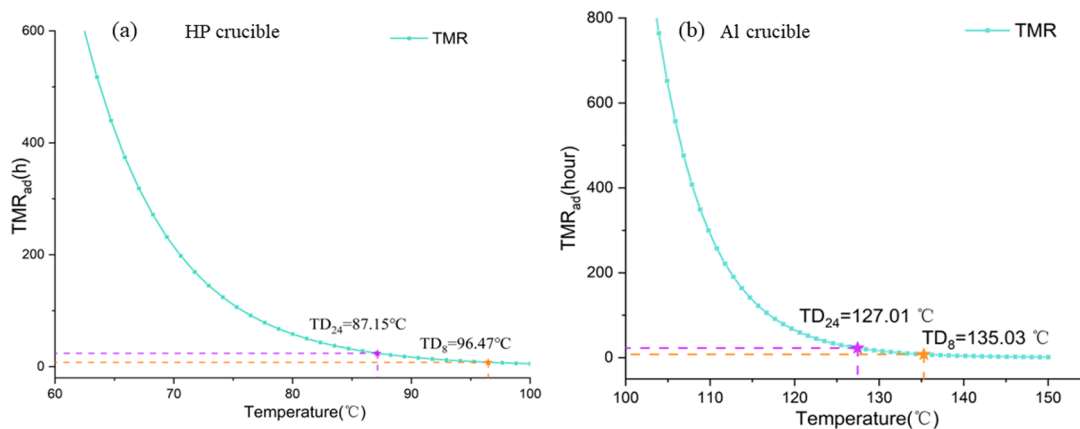


Figure 8. Time to reach maximum rate under adiabatic conditions: (a) HP crucible and (b) Al crucible.

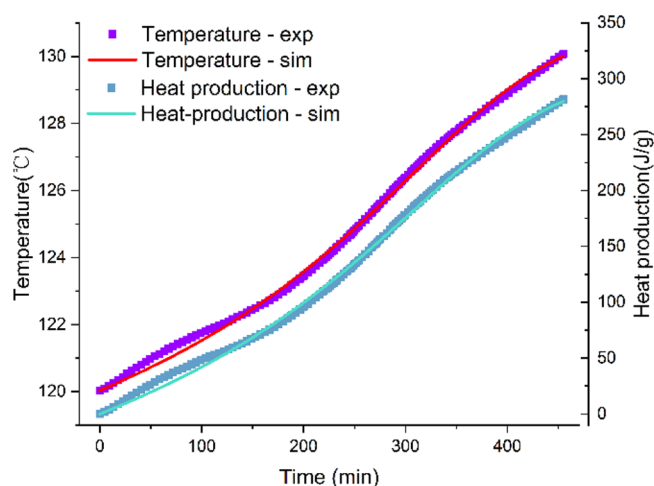


Figure 9. Results of fitting for decomposition temperature and heat production.

objects with nonuniform temperature distributions can be determined.

Initially, when the time is zero, the temperature and transition conditions are set as T_0 and a_{i0} . Additionally, various boundary conditions (BC) must be specified for each surface of an object to solve the heat conduction differential equation effectively. These boundary conditions outline the thermal state at the object's boundary and its interaction with the external environment.

$$\text{BC of the 1st kind: } T|_s = T_e(T) \quad (6)$$

$$\text{BC of the 2nd kind: } q|_s = q_e(t) \quad (7)$$

$$\text{BC of the 3rd kind: } -\lambda \frac{\partial T}{\partial n} \Big|_s = U(T_s - T_e) \quad (8)$$

$$\text{BC of the 4th kind: } -\lambda \frac{\partial T}{\partial n} \Big|_s = \sigma \varepsilon_{\text{eff}} \left(T_s^4 - T_e^4 \right) U(T_s - T_e) \quad (9)$$

where q is the external specific heat flux; n represents the unit outer normal on the boundary; ε_{eff} refers to the effective emissivity; and σ is the Stefan–Boltzmann constant. The subscripts “ s ” and “ e ” indicate parameters associated with the boundary and environment, respectively,

The first kind of boundary condition specifies the temperature on the object's surface. The second kind of boundary condition specifies the heat flux on the object's surface. The third kind of boundary condition specifies the ambient temperature and the heat transfer coefficient (HTC) on the object's surface. The fourth kind of boundary condition includes the third kind plus radiation heat exchange. During the simulation process, the third type of boundary condition is chosen.

Assessing the parameters of thermal explosion hazards is crucial for optimizing the transportation and storage of

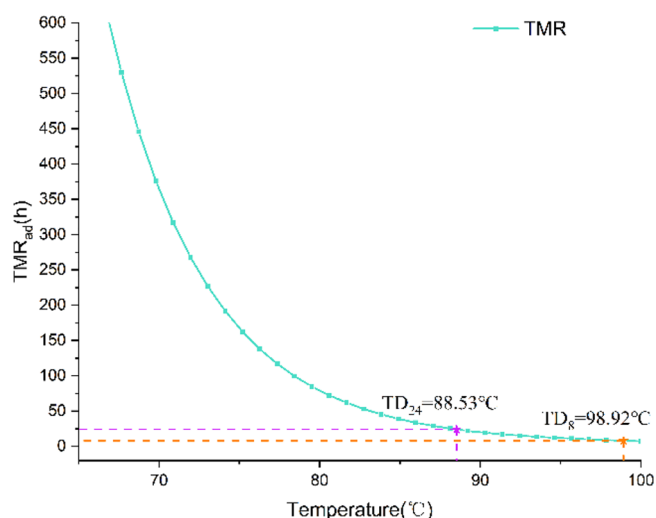


Figure 10. Time to reach maximum rate under adiabatic conditions of reaction mixture.

chemicals and for mitigating industrial risks. These parameters include the self-accelerating decomposition temperature (SADT), control temperature (CT), and emergency temperature (ET).^{22,23} They are derived from numerical calculations of the kinetic model, taking into account the container's geometry and boundary conditions.^{24,25} Separate simulations were conducted for the storage and transportation hazards of DPT in 5, 20, and 50 kg packages, utilizing TSS based on the United Nations SADT test H.4 criteria. The SADT is identified as the lowest ambient temperature at which a temperature increase of at least 6 °C occurs in a specified commercial package within a period of 7 days or less. TSS was utilized to model the storage of DPT in fiberboard barrels, as illustrated in Figure 11a,b. The detailed thermophysical parameters of the samples and their storage containers are detailed in Table 8. The 3D temperature distribution, shown in Figure 11c, reveals an overheating of 6.6 °C at the center when the ambient temperature reaches 66.3 °C in a 20 kg commercial package.

Table 9 displays the predicted results of size parameters and boundary conditions pertinent to different charge quantities and packaging materials in addition to the thermal explosion parameters obtained at 25.0 °C. As the mass of DPT in the package increases, the SADT correspondingly decreases, suggesting that an accumulation of more materials leads to an increased ease in the occurrence of thermal runaway. When comparing various packaging materials, glass containers are observed to be safer with smaller quantities of DPT. As the quality of DPT enhances, the performance of glass and fiberboard converges, whereas polymer packaging materials demonstrate inferior thermal safety.

Under typical conditions, numerical simulations serve as a reliable method for accurately identifying SADT, once specific packaging specifications are established. This Article employs standardized containers and packaging specially designed for

Table 8. Thermal Decomposition Apparent Kinetic Parameters of the Reaction Mixture

stage	$\ln(k_0) \left(\ln \left(\frac{1}{x} \right) \right)$	n_1	n_2	$\ln(z_0)$	E_z kJ/mol	E_a (kJ/mol)	Q (J/g)
1	39.56	1.15	4.12	−0.27	6.32	154.72	170.00
2	−1.35	0.25	0.65	−7.02	2.35	25.016	118.31

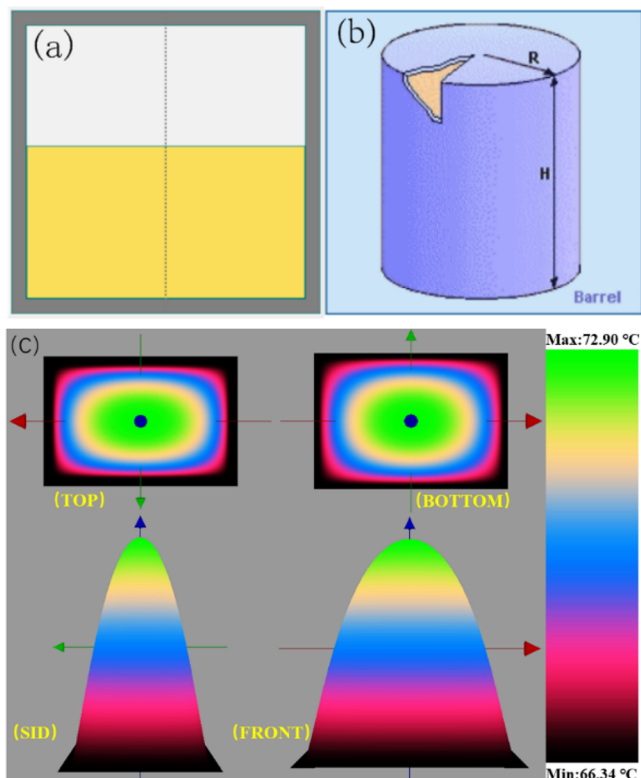


Figure 11. Results of the TSS simulations for SADT include the following: (a) the geometry of the barrel, (b) DPT stored within the barrel, and (c) the 3-D temperature distribution within the material (20 kg, fiberboard barrel).

explosives, adhering to the prescribed specifications. The data obtained provide substantial referential value for manufacturers in practical applications.

4. LIMITATIONS

The principles governing changes in SADT and related data from simulations can be applied to real-world scenarios. It is important to note, however, that these specific values can be affected by factors such as the product purity, environmental humidity, and temperature distribution.

5. CONCLUSIONS

This project assessed the influence of the test environment on DPT's thermal decomposition by employing different types of crucibles. Different heating rates were applied in nonisothermal DSC tests to ascertain the kinetic model and parameters of DPT's thermal decomposition. The primary thermal hazard

parameters of the DPT were obtained. The analysis permits the deduction of several key conclusions.

- 1) The nonisothermal DSC results reveal that DPT's decomposition in the high-pressure sealed crucible encompasses two distinct decomposition phases and seven overlapping exothermic processes (P1–P7). The results of the ARC tests are similar to those observed in the HP crucible, but the observation is less pronounced due to the ample space in the ARC sample bomb. However, in the incompletely sealed Al crucible, only one clearly identifiable decomposition phase is observed, accompanied by a slight endothermic event during the exothermic process. This indicates that utilizing an incompletely sealed aluminum crucible results in the escape of decomposition products and clarifies why the second exothermic process is absent. Comparative experiments demonstrate that careful selection of Al crucibles that cannot be completely sealed is imperative when studying the decomposition reactions of autocatalytic substances to prevent the generation of misleading explanations for the reaction.
- 2) A kinetic-based simulation approach was applied to analyze the nonisothermal DSC data and ARC tests data, determining that the appropriate thermal decomposition kinetic model consists of two phases, encompassing seven autocatalytic stages. Utilizing the dynamic model, the TCL and TMR_{ad} data for DPT were simulated, offering valuable insights for its safe storage.
- 3) To address the issue that data from DSC tests are not directly applicable to real-world scenarios, the thermal hazard parameters, including SADT, for DPT were predicted using the thermal decomposition kinetic model. The study revealed that the SADT of DPT decreases as the mass of DPT in the packaging increases, suggesting that greater material accumulation enhances the possibility of thermal runaway. Investigations were conducted on the impact of various packaging materials on the thermal safety parameters. Results indicated that storing DPT in glassware is safer for smaller quantities, while using fiberboard is preferable for larger masses of DPT.

■ AUTHOR INFORMATION

Corresponding Author

Kun Chen – School of Materials Science and Engineering, Beijing Institute of Technology, Beijing 100811, China; orcid.org/0000-0002-1403-0118; Email: kchen@bit.edu.cn

Table 9. Thermal Hazard Boundary Parameters of DPT

packaging material	mass of sample (kg)	size ($R \times H$) (m)	U ($W/m^2/K$)	void fraction (%)	SADT ($^{\circ}C$)	CT ($^{\circ}C$)	ET ($^{\circ}C$)
fiberboard	5	0.10 \times 0.20	0.20	33.0	74.0	64.0	69.0
	20	0.15 \times 0.30	0.15	28.0	66.0	56.0	61.0
	50	0.20 \times 0.40	0.10	29.0	62.0	52.0	57.0
glass	5	0.10 \times 0.20	1.46	33.0	75.0	65.0	70.0
	20	0.15 \times 0.30	1.20	28.0	66.0	56.0	51.0
	50	0.20 \times 0.40	1.05	29.0	62.0	52.0	57.0
polymer	5	0.10 \times 0.20	0.08	33.0	72.0	62.0	67.0
	20	0.15 \times 0.30	0.06	28.0	65.0	55.0	60.0
	50	0.20 \times 0.40	0.04	29.0	60.0	50.0	55.0

Authors

- Zhi Wang – School of Materials Science and Engineering, Beijing Institute of Technology, Beijing 100811, China
- Shaohua Jin – School of Materials Science and Engineering, Beijing Institute of Technology, Beijing 100811, China; orcid.org/0000-0003-4958-4097
- Guanghui Gu – Gansu Yinguang Chemical Industry Group Co., Ltd., Baiyin 730900, China
- Hui Chao – School of Materials Science and Engineering, Beijing Institute of Technology, Beijing 100811, China
- Shichuan Qian – School of Materials Science and Engineering, Beijing Institute of Technology, Beijing 100811, China
- Yinguang Xu – Gansu Yinguang Chemical Industry Group Co., Ltd., Baiyin 730900, China
- Fan Wang – Gansu Yinguang Chemical Industry Group Co., Ltd., Baiyin 730900, China
- Yulin Wei – Gansu Yinguang Chemical Industry Group Co., Ltd., Baiyin 730900, China
- Xinping Zhao – Gansu Yinguang Chemical Industry Group Co., Ltd., Baiyin 730900, China
- Zhiyan Lu – Gansu Yinguang Chemical Industry Group Co., Ltd., Baiyin 730900, China
- Shusen Chen – School of Materials Science and Engineering, Beijing Institute of Technology, Beijing 100811, China

Complete contact information is available at:

<https://pubs.acs.org/10.1021/acsomega.4c02316>

Notes

The authors declare no competing financial interest.

ACKNOWLEDGMENTS

We are grateful for the financial support of the Beijing Institute of Technology.

REFERENCES

- (1) Choi, C. S.; Bulusu, S. The crystal structure of dinitropentamethylenetetramine (DPT). *Acta Crystallogr. B Struct Crystallogr. Cryst. Chem.* **1974**, *30*, 1576–1580.
- (2) Vagenknecht, J.; Zeman, S. Some characteristics of 3,7-dinitro-, 3,7-dinitroso- and dinitrate compounds derived from 1,3,5,7-tetraazabicyclo[3.3.1]nonane. *Journal of Hazardous Materials* **2005**, *119*, 1–11.
- (3) Xue, M.; et al. Solubility of 3,7-Dinitro-1,3,5,7-tetraazabicyclo [3.3.1] Nonane in Ethanenitrile, Methanol, 1,1-Dichloroethane, Dimethyl Sulfoxide, Acetone, and Mixed Solvents. *J. Chem. Eng. Data* **2015**, *60*, 1683–1687.
- (4) Bachmann, W. E.; Horton, W. J.; Jenner, E. L.; MacNaughton, N. W.; Scott, L. B. Cyclic and Linear Nitramines Formed by Nitrolysis of Hexamine ¹. *J. Am. Chem. Soc.* **1951**, *73*, 2769–2773.
- (5) Tall, A.; Zeman, S. Determination of heats of decomposition of some 1,3,5,7-tetraazacyclooctane and 1,3,5-triazacyclohexane derivatives using differential scanning calorimetry. *J. Therm. Anal.* **1977**, *12*, 75–81.
- (6) Hall, P. G. Thermal decomposition and phase transitions in solid nitramines. *Trans. Faraday Soc.* **1971**, *67*, 556.
- (7) Kruglyakova, L. A.; Stepanov, R. S.; Kekin, Yu. V.; Pekhotin, K. V. Kinetics of Thermal Decomposition of 3,7-Dinitro-1,3,5,7-tetraazabicyclo[3.3.1]nonane. *Russ J. Gen. Chem.* **2019**, *89*, 194–198.
- (8) Duan, X.; et al. Insight into the pyrolysis of 3,7-dinitro-1,3,5,7-tetraazabicyclo [3,3,1] nonan (DPT) based on ReaxFF MD simulations and TG-FTIR-MS techniques. *Fuel* **2023**, *331*, No. 125860.
- (9) Green, S. P.; et al. On the Use of Differential Scanning Calorimetry for Thermal Hazard Assessment of New Chemistry: Avoiding Explosive Mistakes. *Angew. Chem. Int. Ed* **2020**, *59*, 15798–15802.
- (10) Burnham, A. K.; et al. An Appropriate Kinetic Model for Well-Preserved Algal Kerogens. *Energy Fuels* **1996**, *10*, 49–59.
- (11) Jelić, D.; et al. Thermo-Analytical and Compatibility Study with Mechanistic Explanation of Degradation Kinetics of Ambroxol Hydrochloride Tablets under Non-Isothermal Conditions. *Pharmaceutics* **2021**, *13*, 1910.
- (12) Burnham, A. K.; Braun, R. L. Global Kinetic Analysis of Complex Materials. *Energ Fuel* **1999**, *13*, 1–22.
- (13) Kossoy, A.; Benin, A.; Akhmetshin, Y. An advanced approach to reactivity rating. *J. Hazard Mater.* **2005**, *118*, 9–17.
- (14) Wu, W.; et al. Model identification and classification of autocatalytic decomposition kinetics. *J. Therm Anal Calorim* **2023**, *148*, S455–S470.
- (15) Stoessel, D. *Thermal Safety of Chemical Processes: Risk Assessment and Process Design*; Wiley, 2008.
- (16) Vagenknecht, J.; Zeman, S. Some characteristics of 3,7-dinitro-, 3,7-dinitroso- and dinitrate compounds derived from 1,3,5,7-tetraazabicyclo[3.3.1]nonane. *J. Hazard Mater.* **2005**, *119*, 1–11.
- (17) Gorn, M. V.; et al. Pressure DSC for energetic materials. Part 2. Switching between evaporation and thermal decomposition of 3,5-dinitropyrazole. *Thermochim. Acta* **2020**, *690*, No. 178697.
- (18) Roduit, B.; Hartmann, M.; Folly, P.; Sarbach, A.; Baltensperger, R. Prediction of thermal stability of materials by modified kinetic and model selection approaches based on limited amount of experimental points. *Thermochim. Acta* **2014**, *579*, 31–39.
- (19) Roduit, B.; Borgeat, Ch.; Berger, B.; Folly, P.; Alonso, B.; Aebischer, J. N. The prediction of thermal stability of self-reactive chemicals: From milligrams to tons. *J. Therm. Anal. Calorim.* **2005**, *80*, 91.
- (20) Yuan, M. H.; Shu, C. M.; Chen, K. Y.; Kossoy, A. In a study on kinetic model for thermal decomposition of MEKPO by dynamic DSC tests. *Annual Conference of the North American Thermal Analysis Society*, Albuquerque, New Mexico, Sept 22–24, 2003, NATAS, 2003.
- (21) Kossoy, A. More about applying simulation for evaluating reactive hazard of Li-ion battery. *CISP-Newsletter N10 Kinetics-based simulation approach*; CISP, 2016.
- (22) Liu, S. H.; Zhang, B.; Cao, C. R. Assessing the thermal properties of [Bmim]NO₃ through thermokinetic calculations and the energy equilibrium method. *Process Safe Environ.* **2020**, *134*, 270.
- (23) Cao, C. R.; Liu, S. H. Thermal hazard characteristic evaluation of two low-temperature-reactive azo compounds under adiabatic process conditions. *Process Safety and Environmental Protection* **2019**, *130*, 231–237.
- (24) Ren, C.; Liu, H.; Li, X.; Guo, L. Decomposition mechanism scenarios of CL-20 co-crystals revealed by ReaxFF molecular dynamics: similarities and differences. *Phys. Chem. Chem. Phys.* **2020**, *22*, 2827–2840.
- (25) Zhang, J.; Ma, Y.-Y.; Chen, L.-P.; Chen, W.-H. Experimental and numerical simulation to identify the thermal hazards and hazardous scenarios of N-Nitrodihydroxyethyl dinitrate. *Process Safety and Environmental Protection* **2021**, *145*, 211–221.